

Article

Ionospheric Global and Regional Electron Contents in Solar Cycles 23–25

Yury Yasyukevich ^{1,*}, Artem Padokhin ^{1,2}, Artem Vesnin ¹, Alexei Bykov ¹, Alexander Kiselev ¹,
Alexander Ivanov ² and Anna Yasyukevich ¹

¹ Department of Near-Earth Space Physics, Institute of Solar-Terrestrial Physics SB RAS, 664033 Irkutsk, Russia; padokhin@physics.msu.ru (A.P.); artem_vesnin@iszf.irk.ru (A.V.); alexei.bykov@iszf.irk.ru (A.B.); kiselev@iszf.irk.ru (A.K.); annpol@iszf.irk.ru (A.Y.)

² Faculty of Physics, Lomonosov Moscow State University, 119991 Moscow, Russia; ivanov.ak18@physics.msu.ru

* Correspondence: yasyukevich@iszf.irk.ru; Tel.: +7-3952-564-554

Abstract: The Earth’s ionosphere experiences forcing from above and below and varies in different periods. We analyzed the dynamics of the ionospheric global and regional electron contents (GEC and REC) in solar cycles 23/24 (SC23/SC24) and the first part of solar cycle 25 (SC25). We considered several methodological issues for GEC calculations and created a tool to compute GEC and made it available through SIMuRG (System for Ionosphere Monitoring and Research from GNSS). The paper shows the asymmetry of GEC dynamics in different solar cycles. The mid-latitude summer evening anomaly disrupted the diurnal REC variation in the Siberian region under solar minima. The mean GEC showed similar dependence on the F10.7 index in SC25 and SC23/SC24. The difference in solar cycles could prevent reliable forecasting for GEC for the next solar cycle. Our model, based on a neural network, could predict GEC dynamics in SC25 accurately when we input the F10.7 index.

Keywords: ionosphere; global electron content; regional electron content; solar cycle



Citation: Yasyukevich, Y.; Padokhin, A.; Vesnin, A.; Bykov, A.; Kiselev, A.; Ivanov, A.; Yasyukevich, A.

Ionospheric Global and Regional Electron Contents in Solar Cycles 23–25. *Symmetry* **2023**, *15*, 1940. <https://doi.org/10.3390/sym15101940>

Academic Editors: Olga Kodolova, Tomohiro Inagaki and Alberto Ruiz Jimeno

Received: 31 August 2023

Revised: 14 October 2023

Accepted: 17 October 2023

Published: 19 October 2023



Copyright: © 2023 by the authors. Licensee MDPI, Basel, Switzerland. This article is an open access article distributed under the terms and conditions of the Creative Commons Attribution (CC BY) license (<https://creativecommons.org/licenses/by/4.0/>).

1. Introduction

The ionosphere has significant impacts on radio wave propagation and correspondingly on radar, navigation, and communication systems. Many articles have been devoted to studying the Earth’s ionosphere. The Earth’s ionosphere experiences forcing from above and below and varies in different periods. Scientists have investigated regional and local ionospheric processes to create ionospheric models and new ionospheric peculiarities.

Global navigation satellite systems (GNSS) provide global ionospheric maps (GIM) of total electron content (TEC) [1,2]. The GIM were used to study the ionospheric response to magnetic storms [3,4], ionospheric anomalies [5], sudden stratospheric warmings [6], etc. To analyze the general ionospheric pattern, Afraimovich et al. [7] suggested a technique to calculate the global electron content (GEC)—the total number of electrons in the whole ionosphere—and the regional electron content (REC)—over a territory. The technique is based on GIM and currently allows study of the general ionospheric dynamics during more than two solar cycles (1998–2023, solar cycles 23–25).

We built on works by Afraimovich et al. [7] using a bigger dataset (1998–2023) and analyzed global electron content and regional electron content in several regions, based on GIM TEC produced by the CODE (<http://www.cx.unibe.ch>, accessed on 1 August 2023). We studied REC in Siberia (50–55° N, 105–110° E), Europe (50–55° N, 15–20° E), Japan (35–40° N, 135–140° E), Canada (50–55° N, –105––100° E), and Australia (–40––35° N, 135–140° E). The variations in REC and GEC were analyzed, including annual, semi-annual, and 27-day variations. The main aim was to reveal peculiarities in solar cycle 25 compared to previous solar cycles (herein we use the notation SC23, SC24, and SC25 for corresponding

solar cycles). Our motivation was to reveal GEC and REC dynamics linked to hemisphere asymmetry and region asymmetry, to find region-to-region or region-to-world asymmetry.

2. Materials and Methods

Several centers produce global ionospheric maps [8], including JPL, CODE, UPC, CAS, etc. The GIM ingest GNSS data (pseudo range and phase TEC) to obtain total electron content maps. The GIM contain absolute vertical TEC values worldwide (latitude: $-87.5-87.5^\circ$, longitude: $0-360^\circ$) with $2.5 \times 5^\circ$ spatial resolution and 2 h–15 min temporal resolution. We used the final GIM product of CODE (CODG) that is based on the spherical harmonic expansion of TEC spatial distribution [2]. CODG involves the Sun's geomagnetic reference frame and the modified single layer model to obtain vertical TEC values. CODG GIM had 2 h time resolution before 19 November 2014, and 1 h after.

The GIM are freely available through the NASA CDDIS archive (<ftp://cddisa.gsfc.nasa.gov/pub/gps/products/ionex/>, accessed on 1 August 2023). We used the SIMuRG system (<https://simurg.space>, accessed on 1 August 2023) [9] to collect the data and perform calculations. The SIMuRG provides GEC calculations for main GIM products (IGSG, CODG, EMRG, ESAG, JPLG, UPCG, CASG, WHUG), rapid products (UQRG), and model products (C1PG, IRI-2016). The number of products for GIM calculations can be changed.

In the pioneer papers, Afraimovich et al. [7,10] calculated GEC and REC by summing TEC values, I_i , in each cell (over the set of GIM cells), multiplied by the GIM cell area, S_i

$$G = \sum_i S_i I_i, \quad (1)$$

Afraimovich et al. [7,10] used the area at the sea level and indicated that in the absolute value, it could result in a 20% error against electron density integration, but should provide correct variations. If the GEC is used for model correction when you make calculations in a uniform way, the error will disappear.

Earlier, Schaer [2] introduced the very same parameter—the global number of ionospheric electrons—for the peculiar case of GIMs based on spherical harmonics' (SH) expansion within a single thin layer. In this case, mean vertical TEC for global TEC distribution can be represented as a zero-order SH coefficient, C_{00} , given the proper normalization, and thus it is possible to estimate GEC from C_{00} using a simple relation:

$$G = 4\pi(R_E + H)^2 C_{00}, \quad (2)$$

where R_E is the Earth's radius and H is the shell height used in the GIM model.

Schaer's definition [2] is mathematically correct for single shell GIMs based on SH (CODE, WHU, ESA) and differs from Afraimovich et al.'s [7] definition by a factor of $(R_E + H)^2 / R_E^2$. This is one of the reasons why GEC computed according to [7,10] is typically underestimated, which was noted by Gulyaeva and Veselovsky [11]. Gulyaeva et al. [12] used 450 km altitude; this altitude is indicated in GIM and should correspond to the model involved.

Afraimovich's definition of GEC is more common nowadays since it is simple and allows using different GIM even when we do not know SH coefficients. Schaer's approach needs modifications to be applied for multi-shell GIM models (like JPL [13]), tomographic-based approaches (like UPC [14]), or composite IGS GIM [1].

Some alteration to the initial Afraimovich formulation is advisable to make absolute GEC values consistent with Schaer's approach and the results of other models. At the same time, this inconsistency does not affect GEC variations. As for absolute values, one should take special caution to make and use GEC calculations in a uniform (self-consistent) way to avoid possible errors, as well as clearly state the estimation method and type of GIM used in the analysis.

As of now, the SIMuRG system provides the possibility to estimate GEC from different types of GIMs both according to the initial Afraimovich definition and taking into account a correction factor to be consistent with Schaer's definition.

To overcome a problem, one can use global (or regional) mean TEC [15]. Because the factor $(R_E + H)^2/R_E^2$ is common for all GIM cells, it contributes the same in the mean TEC value for different regions. This also allows direct comparison of the ionospheric dynamics in different regions—in this way, the region size does not influence the values. To calculate the global mean TEC, one can use different approaches. The first is to average TEC in GIM

$$\langle I \rangle = \frac{1}{N} \sum_{i=1}^N I_i \quad (3)$$

where N is the number of TEC values in GIM (5112) or in the studied region. The global mean TEC unit is the same as those for TEC—TECU (total electron content unit; 1 TECU = 10^{16} m^{-2}).

The other approach to calculating the global/regional mean TEC is to take into account the weighting factor S_i/S (S_i is the area of a cell, $S = \sum_i S_i$): the area of a GIM cell S_i is the biggest at the equator and decays towards higher latitudes. Introducing the weighting factor allowed us to compare different regions taking into account different areas covered by the same number of GIM cells.

$$\langle I \rangle = \sum_i \frac{S_i}{S} I_i, \quad (4)$$

This approach allowed us to obtain just the parameter C_{00} for GIM based on SH expansion (see above).

Figure 1 shows calculation of the REC based on (4). When a user chose a region (light violet rectangle on the TEC maps), the REC inside the region was calculated using (4). Each global ionospheric map (see the left column) provides a dot (see light violet dots on the right panel) on the REC dynamics. The REC features daily dynamics: equatorial anomaly manifests as stronger during daytime and lighted-enhanced ionosphere increased REC in the day. We could also expect daily variations in GEC due to longitudinal asymmetry [16].

In the third approach (for global electron content, not regional), we expanded GIM into spherical harmonics and used the zero order harmonic coefficient of TEC expansion.

Sometimes it is not easy to understand which approach is used in an article. For example, Hocke [15] and Liu et al. [17] do not show the formula but talk about a simple transformation from GEC to global mean TEC (this indirectly points out that (4) was used).

Using (3) is possible, but is less accurate. Figure 2a shows the dynamics of GEC based on (4) and (3) by red and blue curves, respectively. The curves qualitatively agree for GEC (Figure 2a), but have a bias. When we ignore the fact that the equatorial cells are larger than high-latitude ones, we underestimate mean TEC (TEC at the equator is higher and has greater weight). The difference between (4) and (3) is

$$\Delta \langle I \rangle = \sum_i \left(\frac{S_i}{S} - \frac{1}{N} \right) I_i, \quad (5)$$

Figure 2b shows the REC dynamics in Siberia. Since we used a few GIM cells for calculations, computations using Formulae (3) and (4) were quite similar and the values were almost the same. Figure 2c shows the difference between the weighted mean (4) and just mean (3) $\Delta \langle I \rangle$ for both the entire world (black dots) and Siberia (orange dots). For REC in Siberia, the difference was small—less than 0.4 TECU at the solar maximum (less than TEC estimation error). For GEC at the solar maximum, the difference reached up to 12 TECU, which is quite significant.

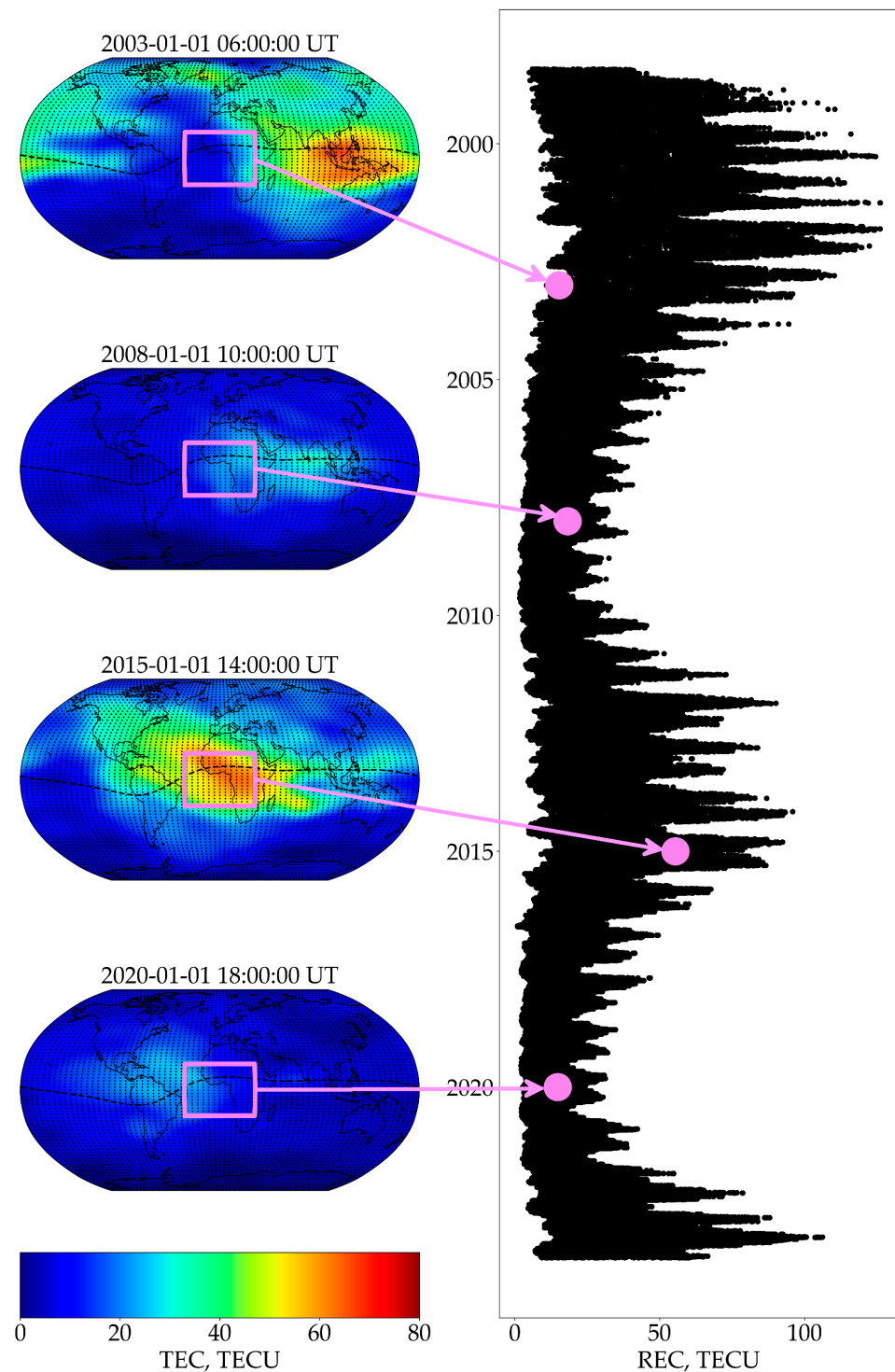


Figure 1. Illustration of REC calculation. Left column shows TEC distribution for 06:00 UT, 1 January 2003; 10:00 UT, 1 January 2008; 14:00 UT, 1 January 2015; 18:00 UT, 1 January 2020. The region for REC is shown by light violet rectangle. On the right panel, the bold dots show corresponding REC, while black dots show general REC dynamics.

For our study, we used the weighted mean (4) to calculate GEC and REC (we preserved these names keeping in mind the simple transformation between the number of electrons and mean TEC).

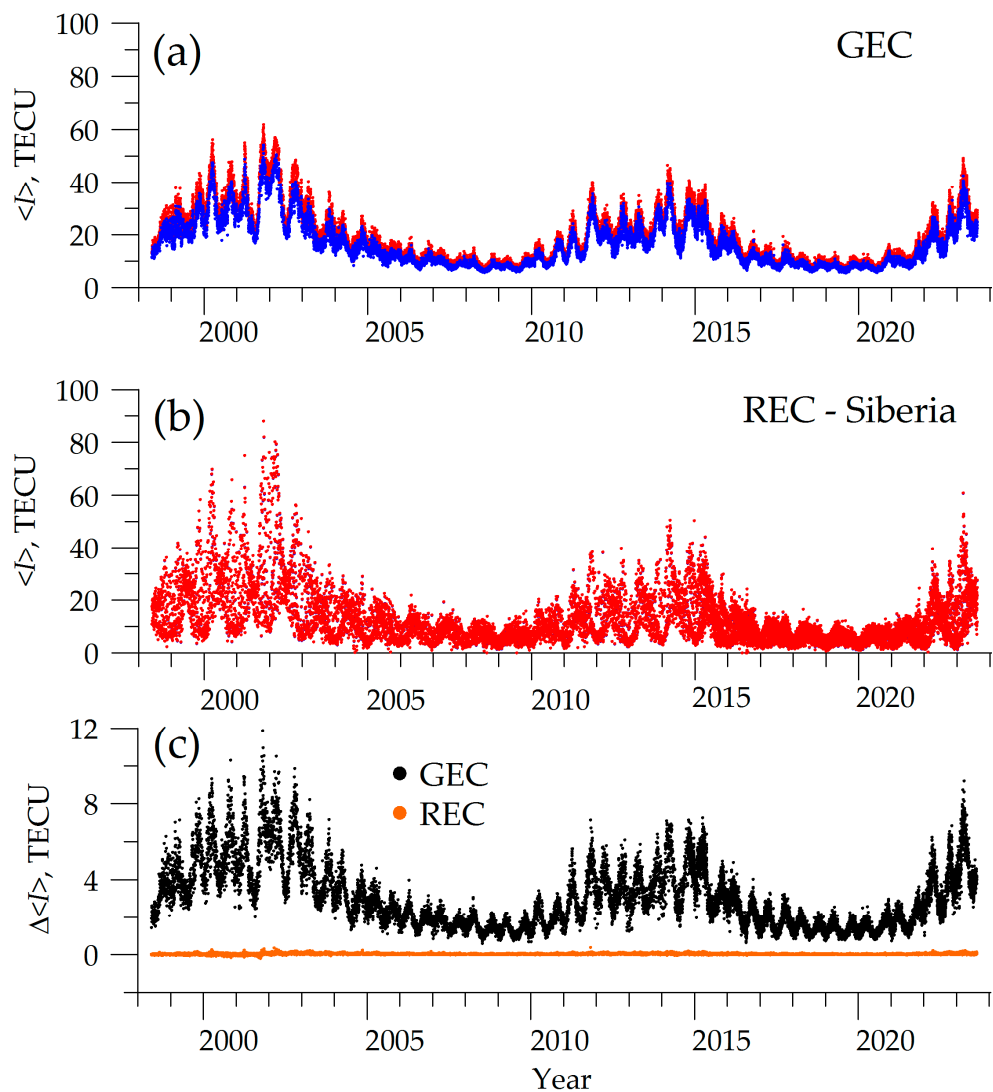


Figure 2. Comparison between the mean and weighted mean TEC: (a) the weighted mean (red dots) and mean (blue dots) TEC throughout the world; (b) the weighted mean TEC in Siberia (red dots); (c) the difference between the weighted mean and the mean TEC throughout the world (black dots) and in Siberia (orange dots).

We used the Butterworth filter with a passband of 200–500 days for annual variations, 100–300 days for semi-annual variations, and 20–40 days for 27-day variations. In the figures, $\langle dI \rangle$ means GEC/REC variations.

We also provided routine treatment of GEC and REC in the SIMuRG (<https://simurg.space/gec>, accessed on 10 October 2023) so researchers could benefit from having such data for their studies. The SIMuRG provides GEC according to Afraimovich [7,10] and Gulyaeva [12] as well as global mean TEC (4).

3. GEC and REC in Solar Cycles 23–25

Figure 3 illustrates the REC dynamics in Siberia, Europe, and Japan, as well as GEC from 1998 to 2023. The thick blue line represents REC data for Siberia; the thin black line, for Europe; the thick gray line, for Japan; the thick black line, for the world, (GEC); the red line, for Canada; and the green line for Australia. In panels (a) and (b), the series are smoothed with a 10-day window to remove diurnal variations; in panel (c), with an 81-day window (to remove diurnal and 27-day variations); in panel (d), with a 365-day window (to reveal general 11-year dynamics). Light blue dots on the background of panel d) represent the F10.7 index (10.7 cm solar radio flux).

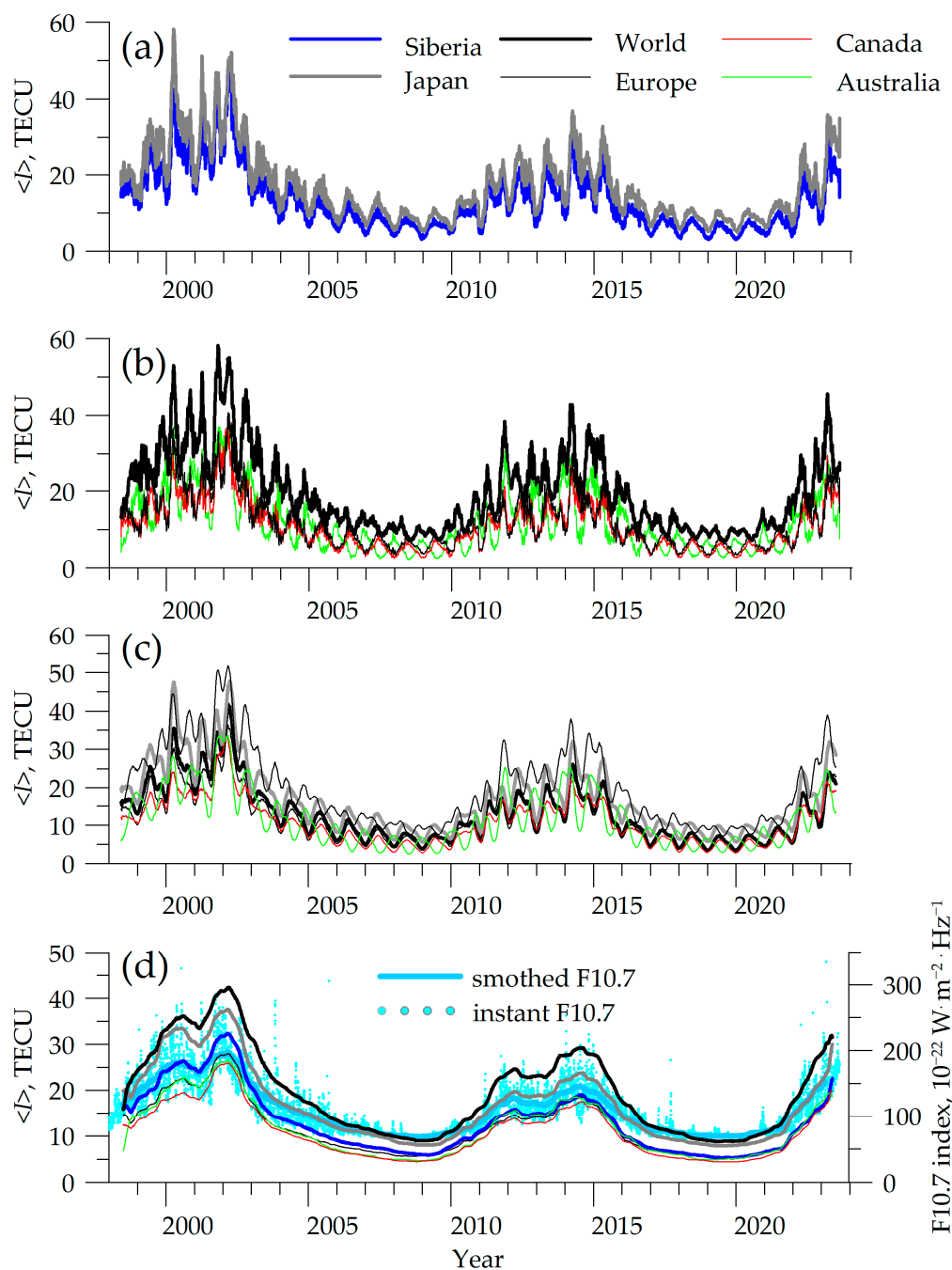


Figure 3. Dynamics of REC in Siberia (blue curve), Europe (thin black curve), Japan (thick gray curve), Canada (red curve), Australia (green curve), and GEC (thick black curve) from 1998 to 2023. In panels (a,b), the series are smoothed with a 10-day window; in panels (c,d) with an 81-day window and a 365-day window, respectively. Light blue dots on the background of panel (d) represent the F10.7 index.

A significant “noise” in data in Figure 3a,b is caused by 27-day variations. The GEC and REC dynamics display annual and semi-annual variations, along with the general 11-year variation describing the solar cycle with solar maximum in 2002. At the same time, the REC in Japan reached higher values in 2000 than those in 2002.

Long-term dynamics of REC and GEC (Figure 3d) reflect the dynamics of solar radio emission (the F10.7 index, blue dots): during SC23, having maxima in 2002 and 2000 with a local minimum in 2001, a significant decrease after 2002 with minima in 2008–2009; during SC24, maxima in 2012 and 2014 with a local minimum in 2013, and a decrease after 2004

with minima in 2019–2020. GEC seems to not to have reached the first maximum in SC25 still. Nevertheless, the current smoothed GEC in SC25 exceeds both maxima in SC24 and tends to have the magnitude of the first maximum of SC23.

REC in Siberia varies over a wide range from 3 to 47 TECU. Maximum values, corresponding to the maximum F10.7 index, were observed in winter 2002. The GEC exceeds the REC in Europe and Siberia. This fact is expected, as near-equatorial regions with high TEC values contribute to GEC but not to European and Siberian RECs.

The smoothed REC in Siberia slightly exceeds that in Europe. In SC23, the difference between them reached ~6–8 TECU, whereas the difference decreases to almost zero in SC24 and SC25. REC in Japan is also higher compared with Europe and Siberia.

Figure 3c shows well-pronounced annual (period ~365 days) and semi-annual variations (period ~180 days). To estimate the magnitude of these variations, we removed trends and variations of different bands. In Figure 4, annual and semi-annual variations are shown in panels (a), (b) and (c), (d), respectively. We used the Butterworth filter with a passband of 200–500 days (for annual variations) and 100–300 days (for semi-annual variations). The thick blue line represents data on REC variations for Siberia. Panels (a), (c), and (b), (d) show data for different regions.

The amplitude of annual REC variations at solar maximum in Japan exceeded that in Siberia. They were fairly similar when solar activity went down and at solar minimum. Annual REC variations (Figure 4b) in Europe and Siberia were almost the same. Maximums of annual REC variations in Siberia were observed in summer, near the summer solstice (this was also true for Japan and Europe). The amplitude of annual REC variations in Siberia gradually decreased from ~6 TECU at solar maxima to 1.5–2 TECU at solar minima.

In 2000–2002, maxima of the annual variations were displaced considerably from summer months. In summer 2002, minimum annual REC variations were observed. In 2000 and 2001, maximum annual REC variations were observed in spring. Amplitude of annual REC variations in Siberia in 2000 was about 7 TECU. The phase of annual variations deviated in 2010 and in 2014.

Annual REC variations in Siberia (and other regions of the northern hemisphere) and annual GEC variations were half-period phase-shifted (Figure 4a,b). Maximum annual GEC variations were observed in winter as well as for the Australian region. This implies that the Southern Hemisphere makes an essential contribution to annual variations. At solar maximum, the amplitude of annual GEC variations is comparable to that of REC variations for all the regions. However, the situation changed after the solar maximum in 2003, when the amplitude of annual GEC variations decreased more than amplitude of annual REC variations. It reflects opposite (half-period shifted) annual variations in different hemispheres, so they partially cancelled each other out.

We see the strongest modulation of annual variation due to the solar cycle for GEC. The modulation is taken as the ratio of annual variation amplitudes on solar cycle maximum and solar cycle minimum. For REC, modulation is smaller: the amplitude of annual variation did not depend on the phase of the solar cycle as much as GEC variation amplitude did.

The amplitude of the semi-annual REC variations (Figure 4c,d) peaked at solar maxima and decreased abruptly at solar minima. The semi-annual REC and GEC variations were in phase. The maximum of semi-annual variations fell on the equinox; the minimum was on the solstice.

In 2000, the amplitude of semi-annual REC variations in Siberia was about 9.5 TECU; in 2002, about 8.5 TECU; from 2004 to 2010, less than 2 TECU. The amplitude of semi-annual GEC variations exceeded that of semi-annual REC variations in Siberia. In 2000, the amplitude of GEC variations was about 12 TECU, whereas it was no more than 1–2 TECU from 2004 to 2009. Semi-annual REC variations in Japan were similar to GEC variations.

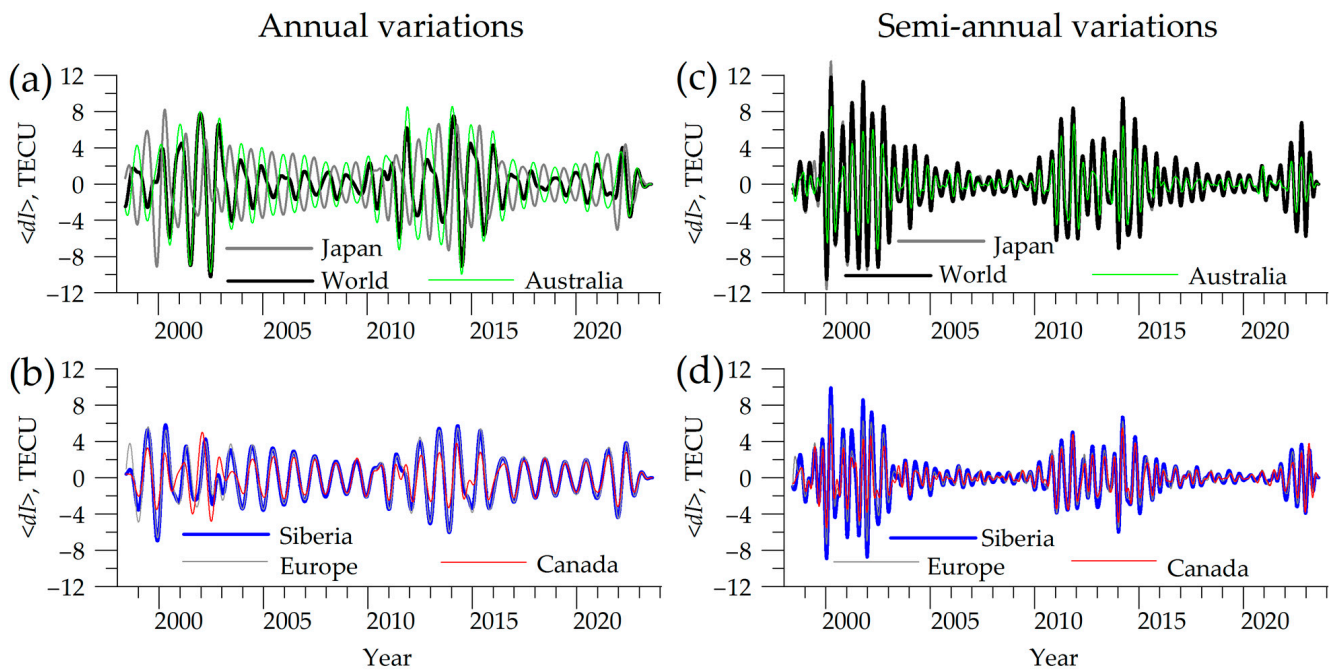


Figure 4. Annual (a,b) and semi-annual (c,d) REC variations in Siberia, Japan, Europe, Australia, Canada, and GEC variations.

We recorded an increase in semi-annual REC/GEC variation amplitude after 2021. However, the amplitude still did not reach that of SC24.

The modulation of semi-annual variations by solar cycle seemed to be stronger than that of annual variations, which is evident from the comparison of left and right panels of Figure 4.

Figure 5a presents 27-day REC variations in Siberia (we show only part of the full interval, from 2008 to 2018, to distinguish peculiarities). The gray curve depicts a 27-day variation envelope. Figures 4c and 5b show 27-day variation envelopes: (b) Europe (thick gray curve), Siberia (thick blue curve); (c) Australia (green curve) and GEC (thick black curve); (d) Canada (red), and Japan (thick gray curve). The amplitude of 27-day variations is modulated. The strongest modulation occurred at a period of ~6 months, though there were harmonics of higher frequencies. At solstices, we observed minimum amplitudes of variations; at equinoxes, maximum amplitudes of variations. The maximum amplitude of 27-day variations was in 2001 (6 TECU in Siberia and 7 TECU in Japan). At solar minimum, the amplitude of 27-day variations was from 0.5 to 2 TECU.

The amplitude of 27-day GEC variations (Figure 5c) from 1998 to 1999 and from 2003 to 2005 exceeded the amplitude of 27-day REC variations in Australia, but not in Siberia/Europe (Figure 5c). These parameters were almost the same for the period from 2000 to 2001.

The amplitude of 27-day REC variations in Europe almost coincided with the amplitude of variations in Siberia. The only exceptions were observed in 2002–2003, when the amplitude of 27-day REC variations in Siberia far exceeded that in Europe and in 2013–2015, when there was a small out-of-the-phase process. Compared with Siberia, 27-day variations in Japan were more significant on average.

We should note that annual and 27-day variation amplitudes did not depend on solar cycle intensity: 27-day variation amplitudes were close in SC23 and SC24.

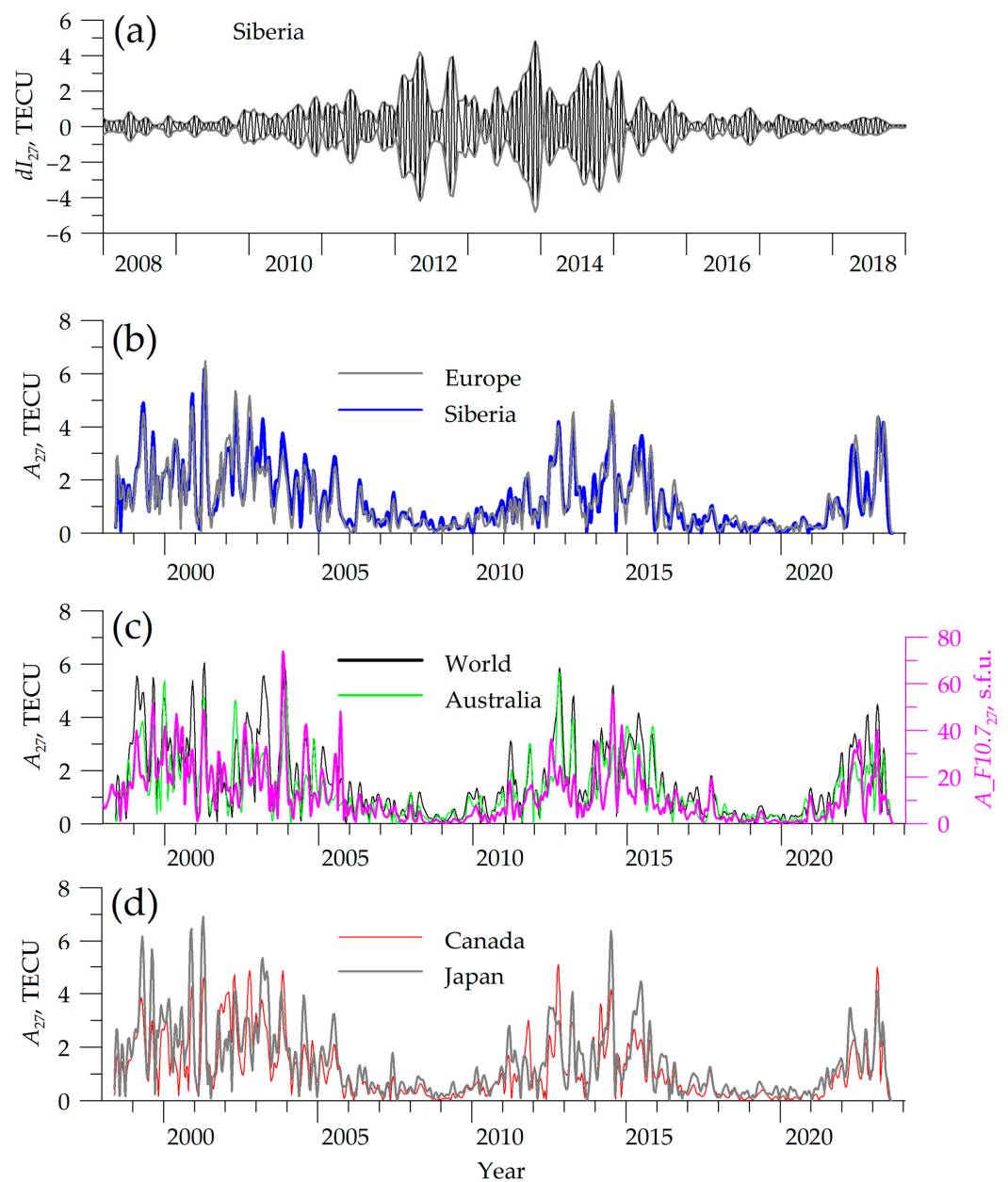


Figure 5. Envelope of 27-day variations. (a) 27-day variations (black line) and their envelope (gray lines) for Siberia; (b) upper envelope of 27-day REC variations in Siberia (blue curve) and Europe (gray curve); (c) upper envelope of 27-day REC variations in Australia (green curve) and of REC variations throughout the world (black curve), and envelope of the F10.7 index variations (magenta); (d) upper envelope of 27-day REC variations in Japan (gray curve) and Canada (red curve).

To analyze diurnal TEC variations, we calculated their amplitude. We compared all values for the chosen day and region with local time, which resulted in averaging the values corresponding to the same local time over the chosen region. The average step was 1 h. The difference between the maximum and minimum values for the given day was taken as the amplitude of diurnal TEC variations.

Figure 6 shows the dynamics of diurnal TEC variations' amplitude. Note that "world" amplitude does not mean "GEC" amplitude because all TECs were chosen in their local time. Panel (a) illustrates the amplitude of diurnal TEC variations in Siberia (thick black curve) and in Europe (gray curve); panel (b), the amplitude of diurnal TEC variations in Japan (gray curve), and throughout the world (black curve).

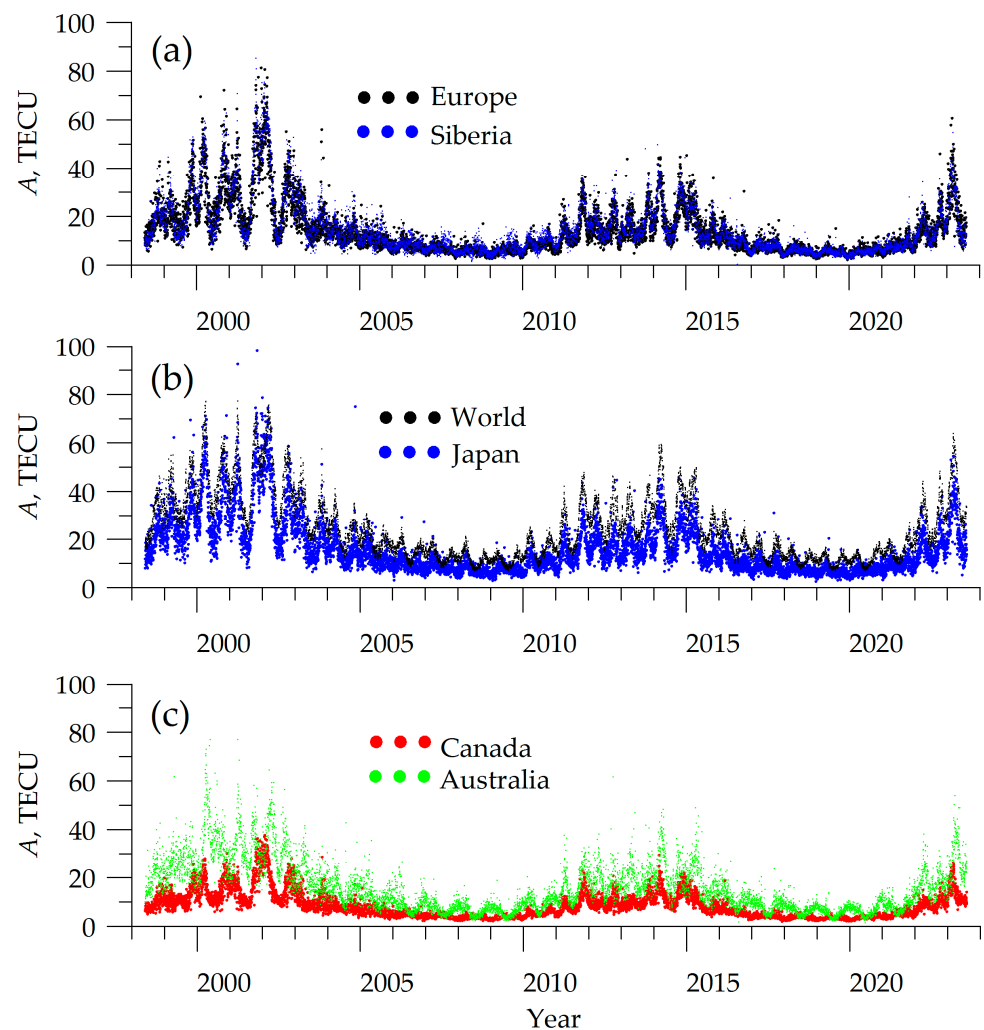


Figure 6. The amplitude of diurnal TEC variations in Siberia (panel (a), blue dots), Europe (panel (a), black dots), Japan (panel (b), blue dots), Canada (panel (c), red dots), Australia (panel (c), green dots), and throughout the world (panel (b), black dots).

The amplitude of diurnal TEC variations was modulated by the annual and 11-year harmonics, as well as by the semi-annual harmonics (to a lesser degree), unlike 27-day variations (see Figure 5), showing the main contributors were semi-annual harmonics and the presence of 11-year harmonics. Curves in Figure 6 resemble those in Figure 3. The mean daily variation amplitude was higher than that of REC, except for the winters in 2000 and 2001, when these magnitudes were comparable. In January 2002, the amplitude of diurnal REC variations in Siberia was ~ 75 TECU.

From 2004 to 2010, these magnitudes were from 1.5 to 30 TECU. By comparison, the amplitude of diurnal TEC variations throughout the world over this period was from 7 to 41 TECU, in Europe, from 3 to 32 TECU, and in Japan, from 3 to 34 TECU (up to 75 TECU in 2004).

Figure 7a,b illustrate dynamics of the daytime (12–13 LT) and nighttime (0–1 LT) REC, respectively. Data series were averaged with a 3-day window to level the extreme events. The black curve presents Siberia; blue dots, Europe. High REC values in Siberia appeared on summer nights. This was most evident at the solar minimum when daytime REC values were quite small. The diurnal variation may become anomalous, and daytime values may become lower than nighttime ones.

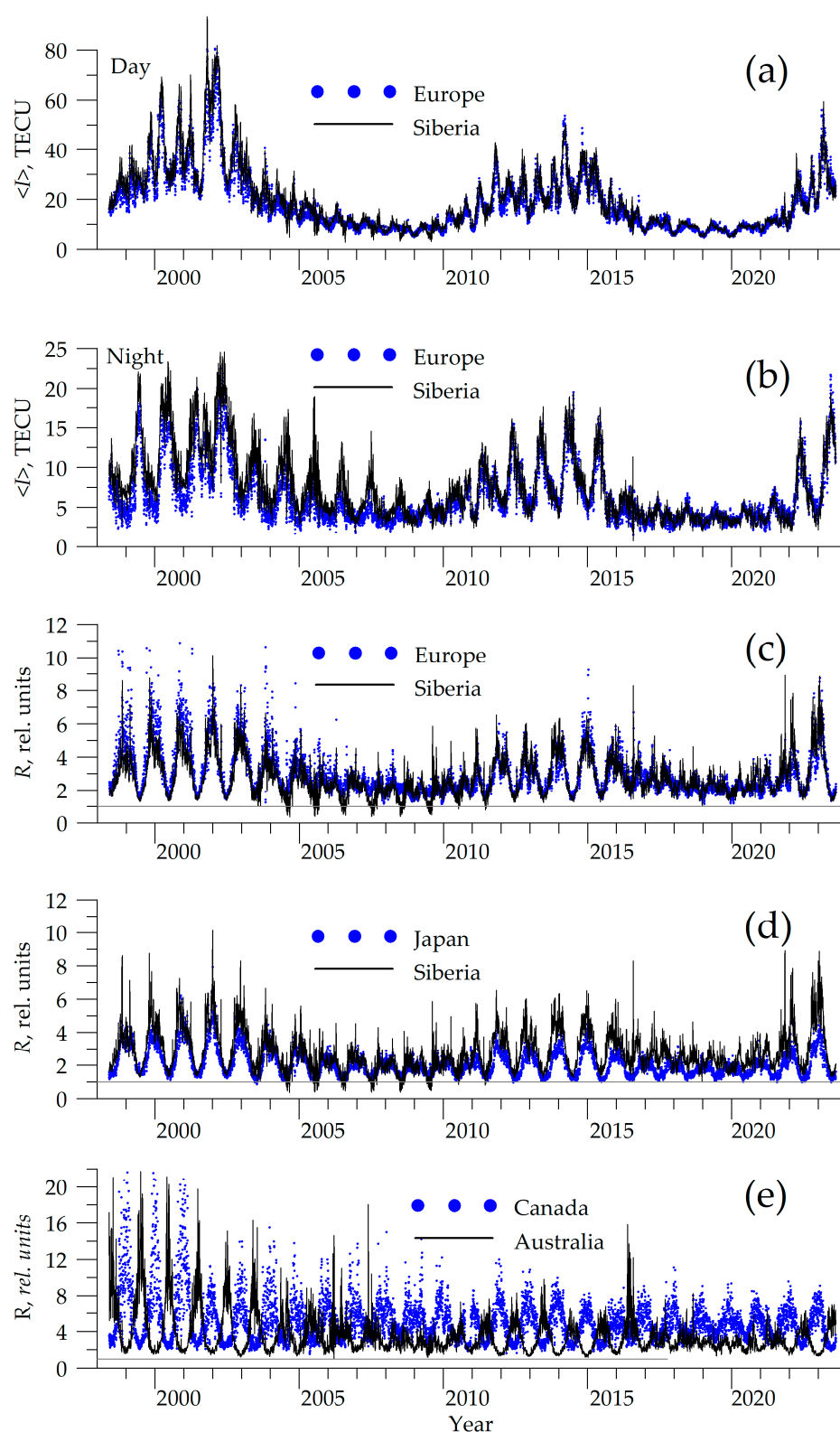


Figure 7. Daytime (a) and nighttime (b) REC in Siberia (black curve) and Europe (blue dots). Panels (c–e) show the ratio of daytime to nighttime REC in Europe ((c), blue dots), Japan ((d), blue dots) and Siberia ((c,d), black curves), Canada ((e), blue dots), and Australia ((e), black curve).

Daytime REC values in Europe and Siberia were almost the same (except for those of summers in 2004–2010). Nighttime REC values in Siberia were much higher. This was most evident in summer, when daytime values are smaller.

To analyze disruption of diurnal variations, we used the ratio of daytime to nighttime REC

$$R = \frac{I_{13}}{I_1}, \quad (6)$$

where I_{13} , I_1 were REC at 12–13 LT and 0–1 LT, respectively.

At high solar activity, R in Siberia can reach 8 (Figure 7c) on certain winter days. Thin black lines indicate $R = 1$, demonstrating when nighttime TEC values were higher than daytime ones. Noteworthy is the fact that R in Siberia in summer has become less than 1 since 2004 (i.e., at solar minimum). This implies that there is a significant disruption of diurnal variations in this region in summer.

As can be seen, R in Europe was close to 2 and varied slightly at the solar minimum. There was a significant dynamic of the ratio of daytime to nighttime ionization in Siberia: R varied from 0.25 to 6. The SC23/SC24 minimum differ from that in SC24/SC25: we did not observe $R < 1$ for the last solar minima.

In Japan, we also observed a dramatic decrease in the ratio of daytime to nighttime ionization during the summer months; they may have become comparable, but daytime ionization was no less than that at nighttime (Figure 7d).

According to [10], GEC values are nonlinearly dependent on solar radio emission at 10.7 cm wavelength. Figure 8 compares GEC and REC in the rising phase of SC25 with those of SC23 and SC24: we chose 3.5 years from the cycle beginning. We see that GEC depends on the F10.7 index in the same way in SC25 and SC24/SC25: the SC25 fit (blue line) is within the SC23/SC24 rise confidence interval (red dashed lines). The same is true for REC in Japan and Australia. Significant differences between the solar cycles are shown for Siberia, Europe, and Canada. We see that SC25 dependencies are more linear for these regions.

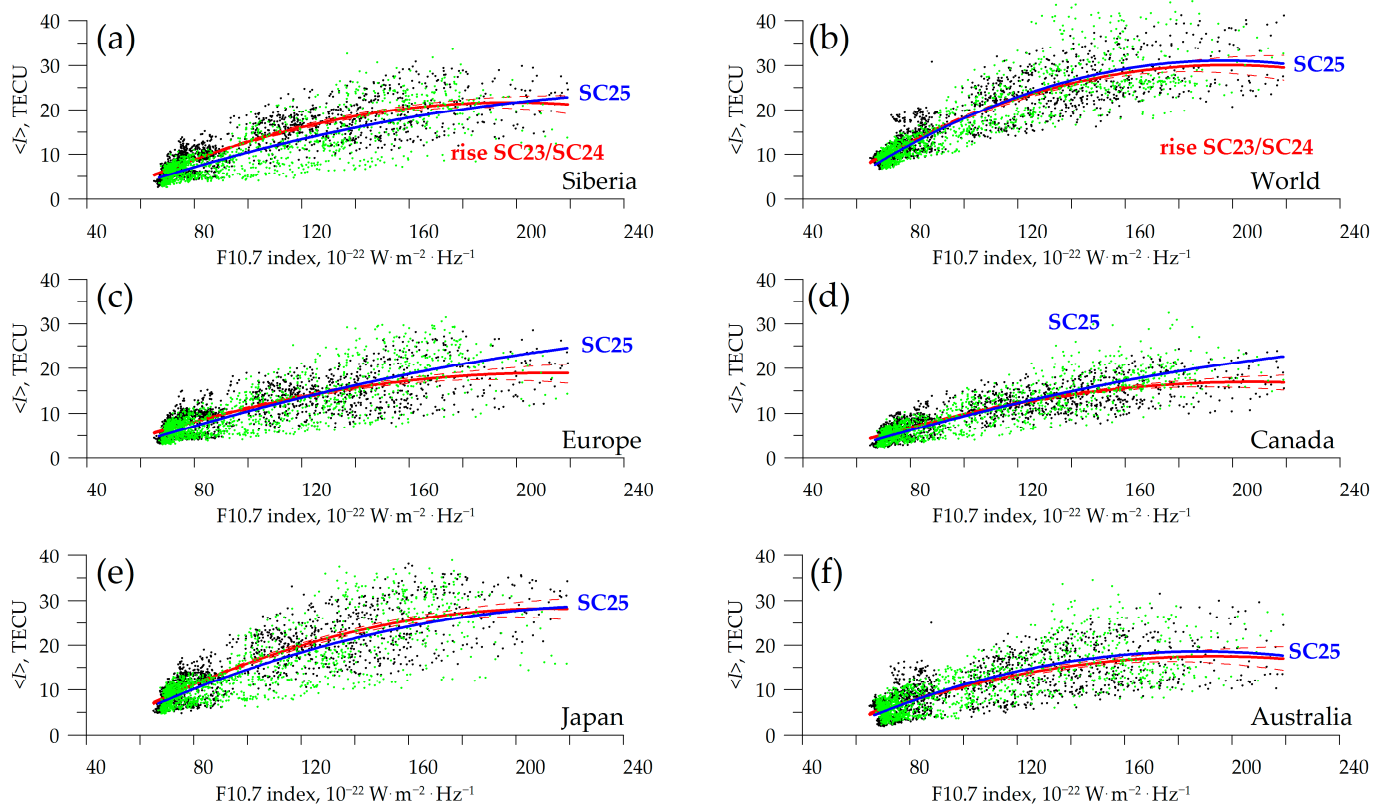


Figure 8. Dependence of GEC (b) and REC in Siberia (a), Europe (c), Canada (d), Japan (e), and Australia (f) on the F10.7 index. Red lines show second-order polynomial fit for the rise of SC23/SC24 (3.5 years from the cycle beginning) and 95% confidence intervals (dashed red lines). The green dots and the blue lines are data and the fits for SC25.

4. Discussion

Many factors influence global and regional ionospheric electron content. GEC and REC are measures of plasma distribution, and plasma can be generated (neutral gas ionization), lost (recombination to neutral gas), and transported. The driver of ionization is solar radiation flux, which must meet particular gas species to produce ionized gas, so the atmosphere composition is also responsible for the ionization/recombination rate. When ionized gas (plasma) is transported to a region of higher/lower recombination, then its gross amount will increase/decrease. Another mechanism that can result in the asymmetry is the long-term trend in the neutral compositions [18,19].

Magnetic pole asymmetry influences GEC/REC asymmetries. The poles of the Earth are very different: the North Pole is in an ocean surrounded by land, while the South Pole is land surrounded by the oceans. This fact leads to the occurrence of sudden stratospheric warmings (that also impact the ionosphere) [6] in the winter in the northern hemisphere, but no comparable events occur in summer in the southern hemisphere. Since we are considering plasma, on top of geographical asymmetry we have asymmetry of different regions in terms of geomagnetic fields. The regions that look similar in terms of the geographic latitude span they occupy (hence the amount of solar ionization radiation they receive is similar, and plasma production is also the same) might be very different in terms of geomagnetic latitude.

An important point is that the magnetic field is changing and the change influences the different processes forming the Earth's ionosphere [20], so this could result in a difference in REC/GEC dynamics in SC23/SC24/SC25.

Magnetic field differences for these regions can cause rather different distributions of plasma (that we study by means of GEC and REC) due to anisotropy: plasma can move along magnetic field lines but not perpendicular to them. This is particularly true for Siberia and Canada: the North magnetic pole is much closer to the latter. The peculiarities in the magnetic field and neutral winds result in the mid-latitude summer evening anomaly (MSEA) [21] and observed disruption (Figure 7) in the classical daily dynamics. Asymmetry in MSEA could be connected with differences in neutral composition in SC23/SC24 and SC24/SC25 solar minima. Most probably it is connected with a weaker vertical gradient of composition (that produces asymmetry in winter-to-summer O/N₂ [22]).

Global and regional electron content could be a proxy to study the asymmetry of the plasma distribution and its temporal variations for different regions. The result shows that in some bands, TEC variations are in phase for both the southern and northern hemispheres. Figure 4 shows that semi-annual variations (period 180 days) are the same for regions in both the northern and southern hemispheres. Semi-annual REC variations are also in phase with GEC, so this allows us to conclude that there are no anomalous regions that show different behavior.

The annual variations show different behavior. Southern regions (Australia) show different behavior to northern ones (Siberia, Japan, etc.). What is more interesting is that the GEC is in phase with annual variations of Australia's REC, which tells us that the Southern Hemisphere should contribute more to annual GEC variations than the Northern Hemisphere. That confirms the findings of [10]. The occurrence of REC maxima for annual variations, in the summer for the Northern Hemisphere region, seems to be as expected: larger sun luminosity results in larger REC.

The Morlet wavelets for GEC, REC, and F10.7 index (Figure 9) show that annual and semi-annual variations are much more significant in the ionosphere than those in the F10.7 index. We also see strong annual variations in solar minima for all RECs. The semi-annual harmonics are absent in the F10.7 index spectra but exist in GEC and REC spectra, which confirms the results shown in Figures 2–5, but visualizes them in a different way.

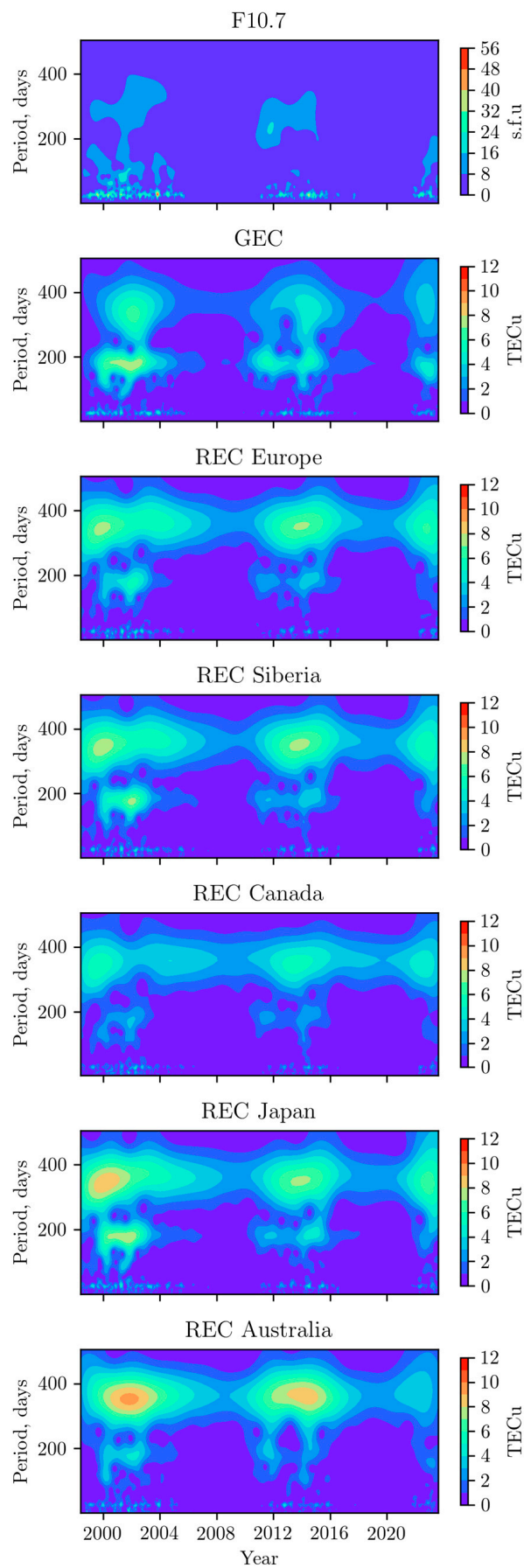


Figure 9. The Morlet wavelets for F10.7 index, GEC, REC in Europe, Siberia, Canada, Japan, and Australia (from top to bottom).

Wavelet coherence [23] of GEC with the F10.7 index (Figure 10) could be treated as a localized correlation coefficient in time frequency space and reveal locally phase-locked behavior of those variations, but not necessarily with high common power. We see almost no correlation for semi-annual harmonics (as expected), but a significant correlation for annual harmonics during solar maxima which rapidly decreases under solar minima. At the same time, the relative phase angle between GEC and the F10.7 index variations differs significantly (up to reversal) even for areas with high observed correlations. At the same time, if those two series are really physically related, we would expect a consistent or slowly varying phase lag. That justifies our conclusions on the prevailing atmospheric rather than solar influence on GEC annual and semi-annual variability. In contrast, for 27-day variations, we observed both high correlations and slowly varying phase angles, suggesting that for those periods the solar activity dominates in GEC variability.

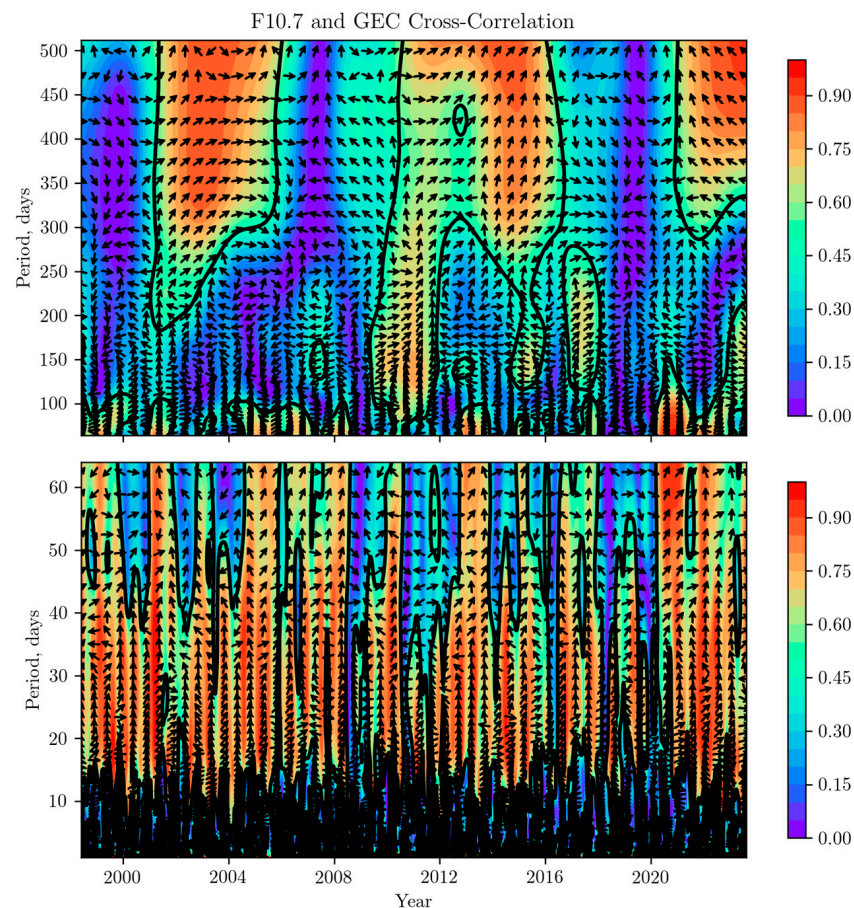


Figure 10. Wavelet coherence for F10.7 index and GEC spectra for 50–500 days (**upper** panel) and 1–65 days (**bottom** panel). Solid black contour lines show 5% significance level against noise. Arrows present relative phase with in-phase pointing up, and anti-phase pointing down.

Figure 8 confirms the results of [24]: there are no significant trends in the global or regional electron contents against solar activity. GEC dependence on F10.7 index is almost the same for SC25 and for SC23/SC24.

Modulation of annual and semi-annual variations during the solar cycle is also not symmetric: it is more pronounced for semi-annual variations than for annual ones. Figure 4 shows that maxima of semi-annual variations fall on equinoxes (spring, autumn) and minima on solstices (summer, winter). This allows us to conclude that the Earth's orientation during the span of the year causes different plasma production rates, which are larger as the sub-solar point is closer to the equator. While Earth revolves, it seems counter-intuitive to see pronounced semi-annual variations; we would expect annual variations to

be more pronounced. However, maxima of semi-annual variation in mid-latitude regions for both Southern and Northern Hemispheres allows us to conclude that it is connected with symmetric plasma production or transport. This also is in agreement with the fact that neutral atmosphere density reaches its maximum values in March and October due to the “thermospheric spoon” [25].

Aframovich et al. [10] supposed that annual and semi-annual variations are too small at solar minima. While this holds for semi-annual variation, annual variations show less pronounced dependence of the amplitude on a solar cycle phase. The symmetry also breaks during the span of the solar cycle. In 2000–2002, the maxima of the annual variations are displaced considerably from summer months to spring. This is not expected, since Earth’s rotation does not depend on the solar cycle, so it is a hint to study other effects; for example, some kind of “memory” or “accumulation” effects when the energy is accumulated during the solar cycle, leading to such a displacement. This accumulation could appear in the atmosphere and reveal non-regular effects such as sudden stratospheric warmings [26].

Figure 11 confirms that annual variations of GEC and REC in regions in the Northern Hemisphere are generally anti-phase, while GEC and REC in regions in the Southern Hemisphere are generally in-phase. Semi-annual variations of GEC and REC in both hemispheres are generally in-phase. This justifies the conclusion of the predominant role of the Southern Hemisphere in GEC annual dynamics. Another feature revealed from these plots is that as we come closer to the maximum of SC25, we begin to observe a noticeable (up to $\pi/2$ absolute value) relative phase shift in annual variations of GEC and REC both for the Northern Hemisphere (positive) and the Southern Hemisphere (negative), which differs SC25 from previous SC24 and SC23.

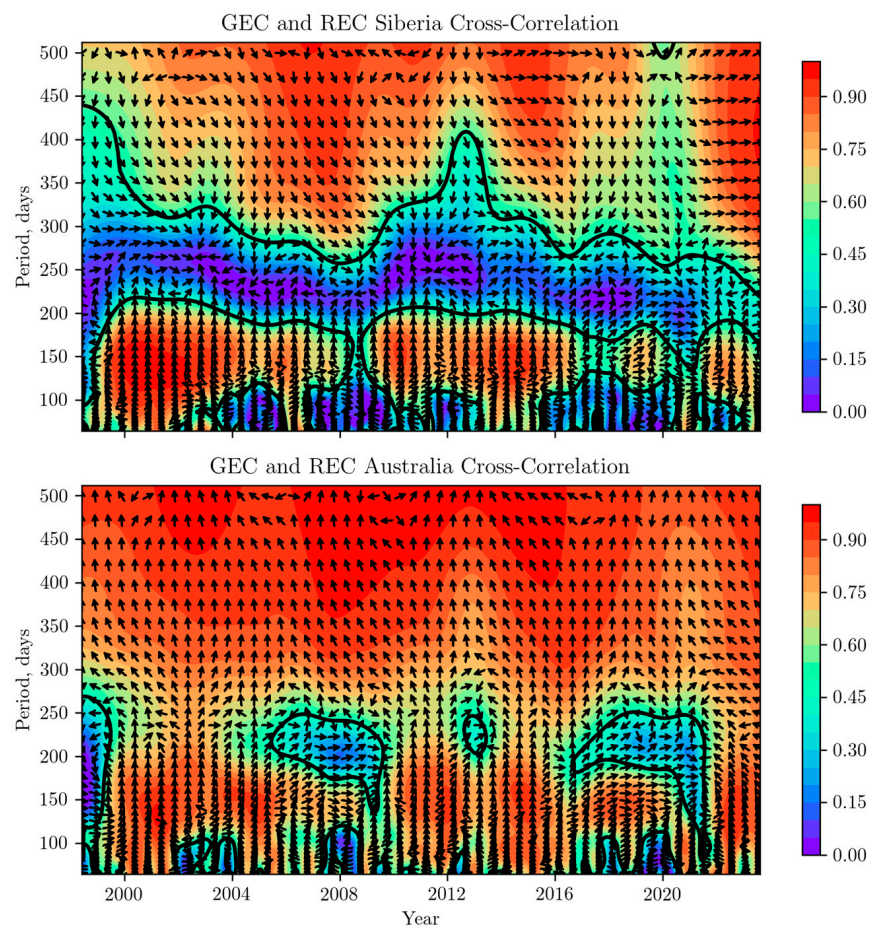


Figure 11. Wavelet coherence for GEC and REC in Siberia (**upper** panel) and Australia (**bottom** panel). Solid black contour lines show 5% significance level against noise. Arrows present relative phase with in-phase pointing up, and anti-phase pointing down.

Chen et al. [27] revealed the difference in the lag of solar cycle (>1 year) variations in extreme ultraviolet and GEC from those in short-term variations (<27 days); so different processes could influence different parts of spectrums.

Afraimovich et al. [7] think that 27-day variations should be maximal at the rising and falling of solar activity rather than at maximum and minimum. Our results show that despite modulation effects, the maximal amplitude of 27-day variations appears on the solar cycle maximum. We see some reduction in 2001 and in 2014—probably due to an increase in modulation amplitude; however, we disagree with previous results on 27-day variations. To the naked eye, the Sun could appear constant. However, it is dynamic systems that could reveal different “power” during different solar cycles.

Figure 5 shows that intensities of 27-day variations are close in SC23 and SC24. This means that the atmosphere dynamics should significantly influence the observed 27-day GEC/REC variations, and probably more significantly than solar flux variations.

We note that the 27-day GEC variations amplitude is modulated by semi-annual harmonic. The question is whether it is due to the changes in solar flux variations or due to the atmosphere dynamics. The envelope of 27-day F10.7 index variations (Figure 5c) also showed modulation that resembles a half-year. Modulation in GEC disagreed with modulation in F10.7 index in the 24th solar maxima (2012–2013, 2015), but for some periods amplitudes agreed. We suppose that at solar maxima, the neutral atmosphere influence is more significant and can outweigh solar flux variation effects.

Some hypotheses exist about the relation of the ionospheric 27-day variations to the ~27 Moon cycle. Bertolucci et al. [28] (who also analyzed 1995–2013 GEC data) studied the combined gravitational effect of the Sun and the Moon.

To check their hypothesis, we calculated maxima in GEC and F10.7 index spectra within 22.5–37 days. Figure 12 shows the dependence of these values for GEC vs. ones for F10.7 index. Most of the data are 24–30 days within gray curves—they show a linear dependence of 27-day variations of GEC on those of F10.7 index. However, on the right part, there is a statistically significant part of the data showing that 27-day GEC variations do not depend on F10.7 index ones. That could be due to other reasons.

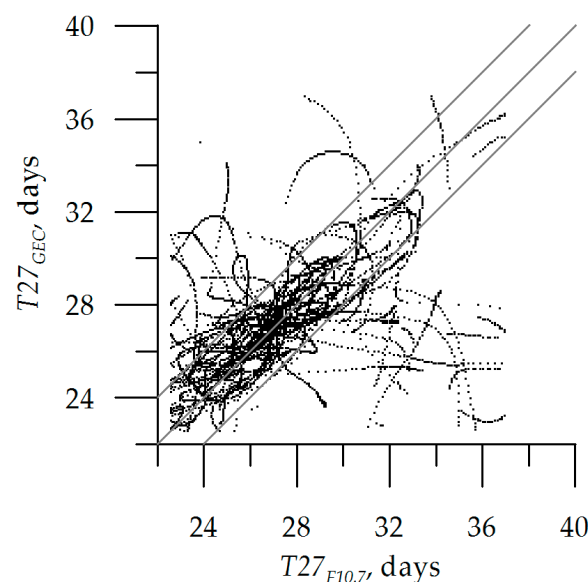


Figure 12. Periods of 27-day variations. Maxima of GEC spectrums within 22.5–37 vs. those of F10.7 index. Slanted gray lines show a 45° slope shifted by $T = 2$ days.

The first reason is the problems/peculiarities in the GIM used for GEC calculation. The second reason is the influence of atmospheric processes preventing solar variations’ impact. We do not think that it could be due to the Moon cycle, because the periods of GEC variation differ (and differ from the Moon cycle).

While we do not suggest any evidence proving or disproving that dark matter can be a factor that influences the ionosphere/thermosphere state (as suggested in [28,29], we hope our data can be involved not only in “traditional” ionospheric research and precise navigation improving, but even in atypical research in the ionosphere physics field.

Figure 3 confirms that solar cycle 25 appears to exceed solar cycle 24, while before we expected that it would be less pronounced. Moreover, taking into account solar cycles 23–24, we could expect the next solar maxima in 2025–2026. Recent papers say that solar cycle 25 will be a little weaker or comparable with solar cycle 24 [30]. Even recent papers say that solar cycle 25 should be a little stronger than the previous one [31]. However, Figure 3 shows that solar cycle 25 is expected to be much higher than solar cycle 24, and we could expect its intensity to be between that of SC23 and SC24—so it will be a much stronger solar cycle that produces a much thicker ionosphere. Since the variations in the ionosphere depend on background, we expect stronger variations in electron density, which could affect such technologies as navigation and radio communication that work through the ionosphere.

Li et al. [32] created a linear storm-time model for the global electron content response. The model requires quiet-time GEC to produce storm-time GEC variations, so it is important to create a background GEC model. We created two neural network-based models for GEC. Both models were fully connected neural networks. The models were taught by Adam optimizer which minimized the root mean square error (RMSE).

We used the 1998–2020 dataset as a training test and performed validation on the same datasets. It was not fully correct, but when we did not try to reach the best quality it was appropriate. For the test set, we used the 2021–2023 dataset.

As inputs, both models (GEC-NN-F10.7-T and GEC-NN-T) used the sin and cos functions of time. The frequencies of functions were chosen to fit characteristic periods: 27 days, 180 days, 365.25 days, and 11 years (4017.75 days). The first model (GEC-NN-F10.7-T) additionally to the mentioned inputs (time information) involved the F10.7 index (so it included the solar cycle). From Figure 8, we could expect that the first model would provide good quality, while from Figure 3 (where we see different time dynamics) we could expect that the second model would not provide the correct GEC dynamics.

We tried different network architectures. For NN-F10.7, a five-layer neural network (10-10-10-10-1) had appropriate quality, while for GEC-NN-T, a two-layer neural network (10-1) showed much less error.

The results are shown in Figure 13. We should note that the models reflected annual and semi-annual variations. The model involving F10.7 index correctly reflected both the increase in solar cycle and the difference in solar cycle and annual/semi-annual variations. The MAE/RMSE were 2.7/3.5 TECU for the model involving F10.7 index, and 4.3/5.3 TECU for the model not involving F10.7 index.

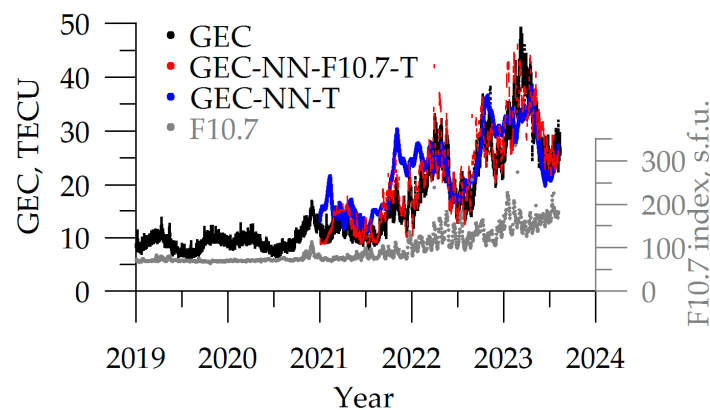


Figure 13. GEC modeling based on neural networks. Black dots show experimental GEC, red dots the neural network model involving the F10.7 index, blue dots the neural network without the F10.7 index, gray dots the F10.7 index.

From Figure 13, we note that without F10.7 index, we underestimated the increase in solar activity and real GEC data.

We took datasets for several solar cycles to cover various time scales: during the span of a year, different regions encounter different conditions in terms of solar ionization flux. Contrary solar cycles mean solar ionization changes and we expect scaling of the effects that appear during the span of a year i.e., quantitative change instead of qualitative. If different behavior is observed, it might be a hint to mechanisms that are not counted (or involved indirectly and nonlinearly).

To check the GEC/REC technique more, we need a separate study for different altitudes, especially above F2. It is not possible with existing GIM. Using information at different altitudes (that could be available using JPL algorithms) would make it possible to perform such a study. It could be useful if GIM also keeps expansion parameters. We are planning to implement this under the SIMuRG project for an algorithm suggested by Padokhin et al. [33].

Our findings in the field of GEC/REC climatology agree with and validate the results obtained in [7,10,34].

5. Conclusions

We performed an analysis of global and regional electron contents and provided a system where users could access this data. Our analysis shows significant asymmetry of GEC and REC dynamics in solar cycles.

The intensity of annual and semi-annual variations follow solar maxima and minima, but the min–max ratio is more significant for semi-annual variations. The 27-day variations in REC and GEC are modulated by semi-annual variations, and an 11-year solar cycle, but do not depend on solar cycle intensity. We did not find a significant decrease in 27-day variations' amplitude in solar maxima, as suggested by other studies.

Annual, semi-annual, and 27-day REC variations in Siberia correlate well with those in Europe. Such correspondence between RECs may be used to study the disruption of “regularity” of REC variations (like we find for Siberia).

A significant disruption of diurnal REC variation in Siberia appears in summer (MSEA), when solar activity goes down. The disproportion of this effect appeared in solar minima of SC23/SC24 and SC24/SC25.

GEC and REC can be used in updating ionospheric models, so we hope that the suggested data will be useful for the ionospheric community. We consider it extremely important to involve the GEC and REC for ionospheric modeling to improve precise navigation, radio location, and communication, and even such unusual fields for ionosphere physicists as dark matter research [28].

The difference GEC/REC dynamics and variations in solar cycles prevent reliable modeling for the next solar cycle and require regular updating of the ionosphere models.

Author Contributions: Conceptualization, Y.Y.; formal analysis, A.V. and A.I., funding acquisition, Y.Y.; investigation, Y.Y., A.P., A.V., A.B. and A.Y.; methodology, Y.Y., A.P. and A.Y.; software, Y.Y., A.V., A.B., A.K. and A.I.; supervision, Y.Y.; validation, Y.Y., A.P. and A.K.; writing—original draft, Y.Y., A.P. and A.V.; writing—review and editing, Y.Y., A.P. and A.V. All authors have read and agreed to the published version of the manuscript.

Funding: The work is financially supported by Russian Science Foundation (project No. 23-17-00157, <https://rscf.ru/project/23-17-00157/>, accessed on 1 August 2023).

Data Availability Statement: GEC and REC data are available through SIMuRG (<https://simurg.space>, accessed on 1 August 2023). Initial CODG data in IONEX format are available through NASA CDDIS (<https://cddis.nasa.gov/archive/gnss/products/ionex/>, accessed on 1 August 2023).

Acknowledgments: We acknowledge CODE for GIM data used for GEC calculations and SIMuRG for data treatment. The GIM data used in this study were acquired as part of NASA's Earth Science Data Systems and archived and distributed by the Crustal Dynamics Data Information System (CDDIS) [35].

Conflicts of Interest: The authors declare no conflict of interest.

References

- Hernández-Pajares, M.; Juan, J.M.; Sanz, J.; Orus, R.; Garcia-Rigo, A.; Feltens, J.; Komjathy, A.; Schaer, S.C.; Krankowski, A. The IGS VTEC Maps: A Reliable Source of Ionospheric Information since 1998. *J. Geod.* **2009**, *83*, 263–275. [[CrossRef](#)]
- Schaer, S. Mapping and Predicting the Earth's Ionosphere Using the Global Positioning System. Ph.D. Thesis, Astronomical Institute, University of Berne, Berne, Switzerland, 1999.
- Buonsanto, M.J. Ionospheric Storms—A Review. *Space Sci. Rev.* **1999**, *88*, 563–601. [[CrossRef](#)]
- Wang, C.; Rosen, I.G.; Tsurutani, B.T.; Verkhoglyadova, O.P.; Meng, X.; Mannucci, A.J. Statistical Characterization of Ionosphere Anomalies and Their Relationship to Space Weather Events. *J. Space Weather Space Clim.* **2016**, *6*, A5. [[CrossRef](#)]
- Yasyukevich, Y.V.; Yasyukevich, A.S.; Ratovsky, K.G.; Klimenko, M.V.; Klimenko, V.V.; Chirik, N.V. Winter Anomaly in NmF2 and TEC: When and Where It Can Occur. *J. Space Weather Space Clim.* **2018**, *8*, A45. [[CrossRef](#)]
- Klimenko, M.V.; Klimenko, V.V.; Bessarab, F.S.; Sukhodolov, T.V.; Vasilev, P.A.; Karpov, I.V.; Korenkov, Y.N.; Zakharenkova, I.E.; Funke, B.; Rozanov, E.V. Identification of the Mechanisms Responsible for Anomalies in the Tropical Lower Thermosphere/Ionosphere Caused by the January 2009 Sudden Stratospheric Warming. *J. Space Weather Space Clim.* **2019**, *9*, A39. [[CrossRef](#)]
- Afraimovich, E.L.; Astafyeva, E.I.; Oinats, A.V.; Yasyukevich, Y.V.; Zhivetiev, I.V. Global Electron Content: A New Conception to Track Solar Activity. *Ann. Geophys.* **2008**, *26*, 335–344. [[CrossRef](#)]
- Roma-Dollase, D.; Hernández-Pajares, M.; Krankowski, A.; Kotulak, K.; Ghoddousi-Fard, R.; Yuan, Y.; Li, Z.; Zhang, H.; Shi, C.; Wang, C.; et al. Consistency of Seven Different GNSS Global Ionospheric Mapping Techniques during One Solar Cycle. *J. Geod.* **2018**, *92*, 691–706. [[CrossRef](#)]
- Yasyukevich, Y.V.; Kiselev, A.V.; Zhivetiev, I.V.; Edemskiy, I.K.; Syrovatskii, S.V.; Maletckii, B.M.; Vesnin, A.M. SIMuRG: System for Ionosphere Monitoring and Research from GNSS. *GPS Solut.* **2020**, *24*, 69. [[CrossRef](#)]
- Afraimovich, E.L.; Astafyeva, E.I.; Zhivetiev, I.V.; Oinats, A.V.; Yasyukevich, Y.V. Global Electron Content during Solar Cycle 23. *Geomagn. Aeron.* **2008**, *48*, 187–200. [[CrossRef](#)]
- Gulyaeva, T.L.; Veselovsky, I.S. Two-Phase Storm Profile of Global Electron Content in the Ionosphere and Plasmasphere of the Earth: Storm Profile of Global Electron Content. *J. Geophys. Res.* **2012**, *117*, A09324. [[CrossRef](#)]
- Gulyaeva, T.; Hernández-Pajares, M.; Stanislawski, I. Ionospheric Weather at Two Starlink Launches during Two-Phase Geomagnetic Storms. *Sensors* **2023**, *23*, 7005. [[CrossRef](#)] [[PubMed](#)]
- Mannucci, A.J.; Iijima, B.; Sparks, L.; Pi, X.; Wilson, B.; Lindqwister, U. Assessment of Global TEC Mapping Using a Three-Dimensional Electron Density Model. *J. Atmos. Sol.-Terr. Phys.* **1999**, *61*, 1227–1236. [[CrossRef](#)]
- Hernández-Pajares, M.; Juan, J.M.; Sanz, J. New Approaches in Global Ionospheric Determination Using Ground GPS Data. *J. Atmos. Sol. Terr. Phys.* **1999**, *61*, 1237–1247. [[CrossRef](#)]
- Hocke, K. Oscillations of Global Mean TEC. *J. Geophys. Res.* **2008**, *113*, A04302. [[CrossRef](#)]
- Klimenko, M.V.; Klimenko, V.V.; Zakharenkova, I.E.; Vesnin, A.M.; Cherniak, I.V.; Galkin, I.A. Longitudinal Variation in the Ionosphere-plasmasphere System at the Minimum of Solar and Geomagnetic Activity: Investigation of Temporal and Latitudinal Dependences. *Radio Sci.* **2016**, *51*, 1864–1875. [[CrossRef](#)]
- Liu, L.; Wan, W.; Ning, B.; Zhang, M.-L. Climatology of the Mean Total Electron Content Derived from GPS Global Ionospheric Maps. *J. Geophys. Res.* **2009**, *114*, A06308. [[CrossRef](#)]
- Laštovička, J. Long-Term Trends in the Upper Atmosphere—Recent Progress. In *Aeronomy of the Earth's Atmosphere and Ionosphere*; Abdu, M.A., Pancheva, D., Eds.; Springer: Dordrecht, The Netherlands, 2011; pp. 395–406, ISBN 978-94-007-0325-4.
- Emmert, J.T.; Picone, J.M.; Meier, R.R. Thermospheric Global Average Density Trends, 1967–2007, Derived from Orbits of 5000 near-Earth Objects. *Geophys. Res. Lett.* **2008**, *35*, L05101. [[CrossRef](#)]
- Dmitriev, A.V.; Suvorova, A.V.; Ghosh, S.; Golubkov, G.V.; Golubkov, M.G. Spatial Evolution of Energetic Electrons Affecting the Upper Atmosphere during the Last Two Solar Cycles. *Atmosphere* **2022**, *13*, 322. [[CrossRef](#)]
- Klimenko, M.V.; Klimenko, V.V.; Ratovsky, K.G.; Zakharenkova, I.E.; Yasyukevich, Y.V.; Korenkova, N.A.; Cherniak, I.V.; Mylnikova, A.A. Mid-Latitude Summer Evening Anomaly (MSEA) in F2 Layer Electron Density and Total Electron Content at Solar Minimum. *Adv. Space Res.* **2015**, *56*, 1951–1960. [[CrossRef](#)]
- Burns, A.G.; Solomon, S.C.; Wang, W.; Qian, L.; Zhang, Y.; Paxton, L.J.; Yue, X.; Thayer, J.P.; Liu, H.L. Explaining Solar Cycle Effects on Composition as It Relates to the Winter Anomaly. *JGR Space Phys.* **2015**, *120*, 5890–5898. [[CrossRef](#)]
- Grinsted, A.; Moore, J.C.; Jevrejeva, S. Application of the Cross Wavelet Transform and Wavelet Coherence to Geophysical Time Series. *Nonlin. Process. Geophys.* **2004**, *11*, 561–566. [[CrossRef](#)]
- Lean, J.L.; Emmert, J.T.; Picone, J.M.; Meier, R.R. Global and Regional Trends in Ionospheric Total Electron Content. *J. Geophys. Res.* **2011**, *116*, A00H04. [[CrossRef](#)]
- Fuller-Rowell, T.J. The “Thermospheric Spoon”: A Mechanism for the Semiannual Density Variation. *J. Geophys. Res.* **1998**, *103*, 3951–3956. [[CrossRef](#)]
- Goncharenko, L.; Chau, J.L.; Condor, P.; Coster, A.; Benkevitch, L. Ionospheric Effects of Sudden Stratospheric Warming during Moderate-to-high Solar Activity: Case Study of January 2013. *Geophys. Res. Lett.* **2013**, *40*, 4982–4986. [[CrossRef](#)]

27. Chen, Y.; Liu, L.; Le, H.; Zhang, H. Discrepant Responses of the Global Electron Content to the Solar Cycle and Solar Rotation Variations of EUV Irradiance. *Earth Planets Space* **2015**, *67*, 80. [[CrossRef](#)]
28. Bertolucci, S.; Zioutas, K.; Hofmann, S.; Maroudas, M. The Sun and Its Planets as Detectors for Invisible Matter. *Phys. Dark Universe* **2017**, *17*, 13–21. [[CrossRef](#)]
29. Zioutas, K.; Argiriou, A.; Fischer, H.; Hofmann, S.; Maroudas, M.; Pappa, A.; Semertzidis, Y.K. Stratospheric Temperature Anomalies as Imprints from the Dark Universe. *Phys. Dark Universe* **2020**, *28*, 100497. [[CrossRef](#)]
30. Chowdhury, P.; Jain, R.; Ray, P.C.; Burud, D.; Chakrabarti, A. Prediction of Amplitude and Timing of Solar Cycle 25. *Sol. Phys.* **2021**, *296*, 69. [[CrossRef](#)]
31. Espuña Fontcuberta, A.; Ghosh, A.; Chatterjee, S.; Mitra, D.; Nandy, D. Forecasting Solar Cycle 25 with Physical Model-Validated Recurrent Neural Networks. *Sol. Phys.* **2023**, *298*, 8. [[CrossRef](#)]
32. Li, S.; Galas, R.; Ewert, D.; Peng, J. An Empirical Model for the Ionospheric Global Electron Content Storm-Time Response. *Acta Geophys.* **2016**, *64*, 253–269. [[CrossRef](#)]
33. Padokhin, A.M.; Andreeva, E.S.; Nazarenko, M.O.; Kalashnikova, S.A. Phase-Difference Approach for GNSS Global Ionospheric Total Electron Content Mapping. *Radiophys. Quantum Electron.* **2022**, *65*, 481–495. [[CrossRef](#)]
34. Younas, W.; Amory-Mazaudier, C.; Khan, M.; Amaechi, P.O. Climatology of Global, Hemispheric and Regional Electron Content Variations during the Solar Cycles 23 and 24. *Adv. Space Res.* **2023**, *71*, 16–28. [[CrossRef](#)]
35. Noll, C.E. The Crustal Dynamics Data Information System: A Resource to Support Scientific Analysis Using Space Geodesy. *Adv. Space Res.* **2010**, *45*, 1421–1440. [[CrossRef](#)]

Disclaimer/Publisher’s Note: The statements, opinions and data contained in all publications are solely those of the individual author(s) and contributor(s) and not of MDPI and/or the editor(s). MDPI and/or the editor(s) disclaim responsibility for any injury to people or property resulting from any ideas, methods, instructions or products referred to in the content.